ADVANCED FUNCTIONAL MATERIALS
www.afm-journal.de

Unveiling the Mechanism of Water-Triggered Diplex Transformation and Correlating the Changes in Structures and Separation Properties

Li-Hui Cao, Yong-Sheng Wei, Hong Xu, Shuang-Quan Zang, and Thomas C. W. Mak*

Recently, great attention has been devoted to the initial and final structures of single-crystal to single-crystal (SCSC) transformations and dissolution-recrystallization structural transformations (DRSTs), whereas the isolation and characterization of crucial intermediates and the unequivocal mechanism of the dynamic conversion process receive comparatively little consideration. Herein, a Cu^{II}-based porous coordination polymer (PCP), which possesses a Kagomé lattice, is solvothermally synthesized. Triggered by water, the 2D Kagomé lattice (PCP-1) primarily undergoes a reversible SCSC transformation to a distorted Kagomé intermediate (PCP-2), which is followed by a DRST process to form a 3D NbO framework (PCP-3) in situ. To the best of our knowledge, this is the first demonstration of a mixed SCSC and DRST transformation process. Notably, the sequential transformations result in the formation of the intermediate and the final product, which could not be obtained by direct synthesis. Regarding the intermediate, we have characterized the transformation separately and propose a plausible mechanism. More interestingly, the adsorption isotherms of water, methanol, and ethanol for the activated materials are distinctly different from one another. PCP-2′ can uptake all three vapors with different adsorption capacities; however, the 3D transformed material PCP-3′ only significantly absorbs water, which is concomitant with an amorphous-to-crystalline transformation, leading to the selective extraction of water from alcohol.

1. Introduction

Porous coordination polymers (PCPs) are intriguing hybrid materials that have potential applications in catalysis, sensing, gas storage and separation, ferroelectricity, proton conduction, etc.[1–6] One of the most successful strategies for constructing PCPs is to use metal carboxylate clusters with well-defined geometries to serve as secondary building units (SBUs) of topological networks.[7,8] In the past decades, a family of PCPs based on the paddle-wheel $M_2(RCO_2)_4(L^T)_2$ cluster component (where M is a transition metal cation, RCO_2 an organic carboxylate, and L^T a terminal anionic or solvato ligand) has been widely studied.[9] Usually, paddle-wheel-based PCPs constructed by modifying the organic linkers can exhibit different dimensionalities and functionalities, as well as topologies including Kagomé lattice, **nbo**-, **pcu**-, **stp**-, and **rht**-based nets.[10]

Recently, flexible porous frameworks have attracted much attention because they usually exhibit dynamic behavior and structural transformation, which can be triggered by heat, light, mechanochemical stimuli, and changes in guest molecules.[11–15] The structural transformation of coordination polymers always involves the breaking and re-making of coordinated or covalent bonds, and some novel structures that cannot be synthesized under conventional conditions may be obtained through structural transformation processes.[16,17] Among the structural transformations of PCPs, two types can be identified, namely, solid-state structural transformations (SSSTs)[18–21] and dissolution-recrystallization structural transformation (DRSTs).[22] In particular, SCSCs,[23–27] which are the most important subset of SSSTs, and DRSTs are highly desirable to identify the structural changes by single-crystal X-ray crystallography.[28] To date, a large number of transformation reports have focused on studies of the initial and final structures of the SCSC or DRST. However, the mechanism of the dynamic process and the intermediates of the structural conversion remain largely unexplored.[27,29,30]

Generally, structural transformations can result in changes in the coordination number, geometry, dimensionality, and inter-penetration.[31,32] Especially, dimensionality changes of coordination polymers are more interesting because they are often accompanied by drastic changes in physical and chemical properties. For example, the groups of Kitagawa[25] and Vittal[18] reported a series of peculiar structural transformations between 2D and 3D structures using different external stimuli. More importantly, these studies revealed the structure–property relationships of crystalline materials, and demonstrated that porous coordination polymers have huge potential in the

L.-H. Cao, Dr. Y.-S. Wei, Prof. H. Xu, Prof. S.-Q. Zang, Prof. T. C. W. Mak
College of Chemistry and Molecular Engineering
Zhengzhou University
Zhengzhou 450001, P. R. China
E-mail: zangsqzg@zzu.edu.cn
Prof. T. C. W. Mak
Department of Chemistry and Center of Novel Functional Molecules
The Chinese University of Hong Kong
Shatin, New Territories, Hong Kong SAR, P. R. China

DOI: 10.1002/adfm.201503154

© 2015 WILEY-VCH Verlag GmbH & Co. KGaA, Weinheim

separation of gases or solvents. As water, methanol, and ethanol always form an azeotrope owing to their similar chemical properties, separation of water from its mixtures with alcohol still poses a big challenge in chemical industry.[33,34] Because PCPs are possible energy-efficient materials by virtue of their designable pore structures and high surface areas, they are expected to play an effective role on the selectivity and uptake capacity of such small molecules, especially for trace quantities thereof.[35]

In this work, we demonstrate an unprecedented water-triggered structural transformation involving both SCSC and DRST processes from a common 2D Kagomé lattice to a 3D NbO framework with a distorted Kagomé structure as the intermediate, accompanied by an unusual pore regeneration and dimension alteration. To the best of our knowledge, to date there have been no other examples of transformation processes that involve both SCSC and DRST transformations. More importantly, we have isolated the distorted Kagomé lattice intermediate during the dynamic conversion, which motivates us to better understand the unique structural transformation. In addition to clarifying the transformation processes separately and in detail and proposing a reasonable mechanism for the conversion, we also studied the gas-adsorption properties for the activated materials before and after structural transformation. The desolvated 2D Kagomé network can uptake the vapors of water, methanol, and ethanol with diverse adsorption capacities; however, the activated 3D NbO framework only selectively absorbs water vapor, resulting in a remarkable separation of water from alcohol.

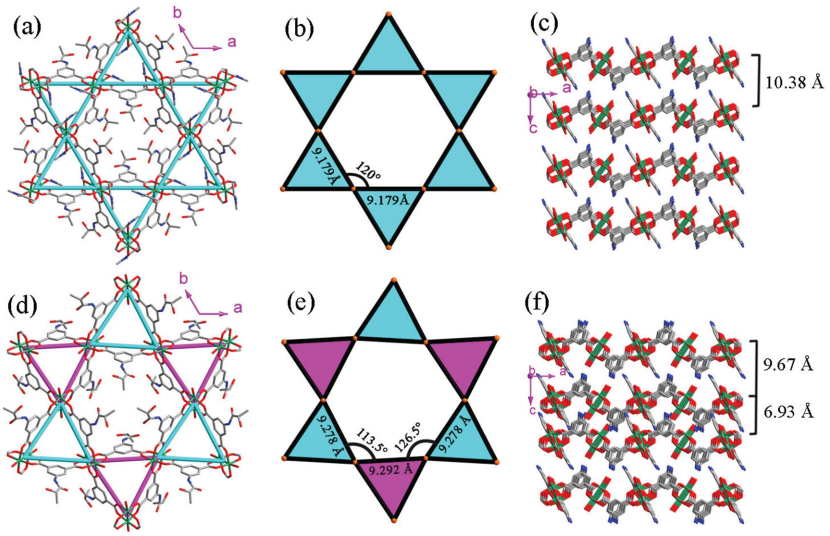

Figure 1. a) Standard 2D Kagomé lattice of PCP-1. b) Nodes indicating the distance and angle of the Cu^{2+} paddle-wheel units in PCP-1. c) Stacking in an *AAAA* fashion of the Kagomé-type PCP-1 structure. d) Distorted 2D Kagomé lattice of PCP-2. e) Nodes indicating the distances and angles of the Cu^{2+} paddle-wheel units in PCP-2. f) Stacking in an *ABAB* fashion of the distorted Kagomé-type PCP-2 structure. All hydrogen atoms are omitted for clarity, and branched chains are also omitted in (c) and (f).

2. Results and Discussion

2.1. Synthesis and Structures of PCPs

Solvothermal reaction of copper(II) nitrate with 5-(2-acetoxy-propionylamino)-isophthalic acid (H_2L) in a 2:1 volumetric mixture of *N,N′*-dimethylacetamide (DMAc) and H_2O at 90 °C yields green hexagonal flake crystals of $[Cu(L_1)(DMAc)]_n$ (PCP-1, H_2L_1 = 5-(2-hydroxy-propionylamino)-isophthalic acid) (see Experimental Section). The acetyl group plays an important protection–complexation–deprotection[36] role in this process, because PCP-1 cannot be synthesized directly by using H_2L_1 instead of H_2L. Single-crystal X-ray analysis (SCXA) showed that PCP-1 belongs to the trigonal space group $P\bar{3}$. The asymmetric unit consists of one Cu^{2+} ion, one L_1^{2-} ligand, and one coordinated DMAc molecule. Interestingly, the Cu^{2+} ions and L_1^{2-} ligands form binuclear copper paddle-wheel units that have 4-connected vertices, and the axial positions are occupied by DMAc molecules (Figure S3a, Supporting Information). In this case, binuclear copper SBUs are bridged by the L_1^{2-} ligands to afford a 2D coordination network along the *ab* plane with a 4-connected standard Kagomé topology (see **Figure 1**a). In the Kagomé layer, every hexagon with S_6 symmetry is encircled by six equilateral triangles (atom-to-atom distance; ca. 9.179 Å) with C_3 symmetry (Figure 1b). The sheets are stacked directly on top of each other with a separation distance of 10.38 Å (the length of the *c* axis, Table S1, Supporting Information) to form the final 3D supramolecular structure (Figure 1c). There are two types of pores in the extended framework of PCP-1. The triangular channels filled with DMAc molecules are made up by three paddle-wheel SBUs and three L_1^{2-} ligands, and the hexagonal pores with "closed doors" are hydrophobic in nature as they contain six 2-hydroxy-propionylamino groups inside, three of which point down and the other three point upwards. It is important to mention that removal of the DMAc molecules that are coordinated on the Cu^{II} would result in unsaturated copper sites and triangular hydrophilic channels. The potential void space of the structure, as calculated by PLATON software,[37] was found to be 1617.9 $Å^3$, which is approximately 53.4% of the unit cell volume.

As shown in **Scheme 1**, when PCP-1 was immersed in water for 10 minutes at room temperature, the coordinated DMAc molecules could be totally replaced by water, and then the intermediate $\{[Cu_2(L_1)_2(H_2O)_2]\cdot H_2O\}_n$ (PCP-2) was obtained. The crystal data for PCP-2 were of poor quality, with unsatisfactorily high *R* factors, which may be due to the disordered coordinated solvent molecules and imperfection in the crystalline-state ligand exchange process. The electron-density maps (2Fo-Fc) indicate that the electron distribution around Cu^{II} paddle-wheel units is more symmetric in PCP-1, but severely deformed in PCP-2, which may be the result of the disordered coordinated solvent molecule (Figure S5, Supporting Information). However, this does not affect the determination of its crystal structure and putative transformation mechanisms. The host-framework of PCP-2 shows the same space group ($P\bar{3}$) and

© 2015 WILEY-VCH Verlag GmbH & Co. KGaA, Weinheim

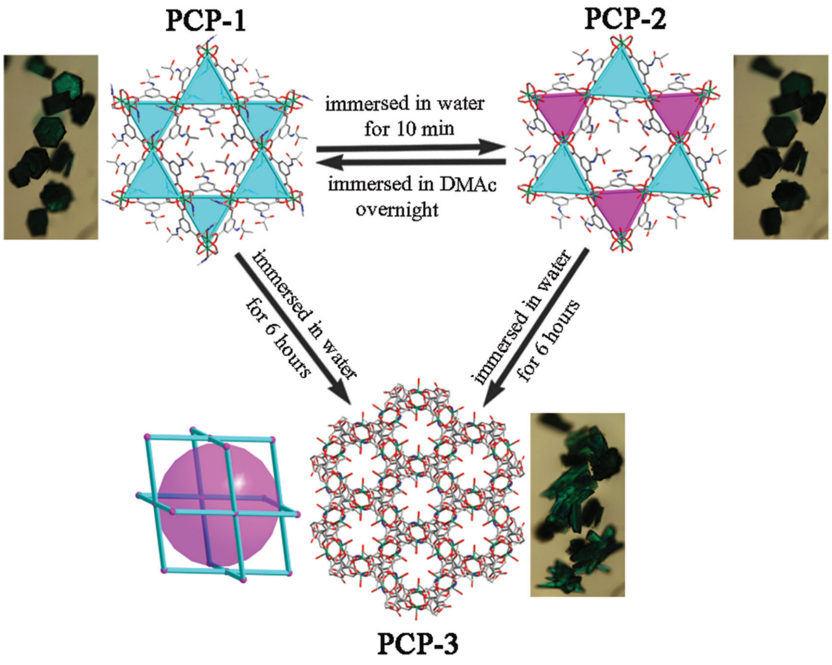

Scheme 1. Structural transformations of the copper(II)-based materials. The insets are microscopic pictures of the water-mediated transition.

metal-ligand connectivity as PCP-1. On the other hand, its asymmetric unit, unlike that in PCP-1, consists of two copper(II), two L_1^{2-} ligands designated as model I and II (Figure S3b and S4, Supporting Information), and two coordinated water molecules. As shown in Figure 1d and 1e, a careful examination of the relative positions of the Kagomé layers revealed that two different distances (9.292 Å for model I and 9.278 Å for model II) and angles (113.5° and 126.5°) were found for the distorted hexagon. PCP-2 differs from PCP-1 in terms of the coordination of the solvent molecules with the Cu paddle-wheel SBU (Figure S3a and S3b, Supporting Information) and of the overall structure packing (Figure 1c and 1f). 2D compounds with Kagomé topology usually pack in an *AAAA* fashion; however, PCP-2 packs in an unusual *ABAB* fashion along the direction of the crystallographic *c* axis. Two independent L_1^{2-} ligands in the same layer lead to different interlayer separations between adjacent layers (9.67 and 6.93 Å, Figure 1f), and the sum of the two distances is nearly equal to the length of *c* axis (16.56 Å, Table S1, Supporting Information). The potential void space of the crystal was found to be 1477.9 $Å^3$, which is approximately 31.0% of the unit cell volume.

Remarkably, after being immersed in water for 6 hours, crystalline PCP-1 or PCP-2 underwent a visible shape change from a hexagonal to a strip-like morphology (see Scheme 1 and Video S1, Supporting Information). SCXA of this final product revealed the formation of a new crystalline species formulated as $\{[Cu(L_1)(H_2O)\cdot 2H_2O]\}_n$ (PCP-3) with a distinctive 3D NbO framework. That is to say, the 2D coordination network can undergo a spontaneous DRST process in water. It is worth noting that PCP-3 crystals cannot be obtained directly by the treatment of H_2L or H_2L_1 with Cu^{II} salts [for example, $Cu(NO_3)_2$, $CuCl_2$, $Cu(ClO_4)_2$ or $Cu(OAc)_2$]. Unlike PCP-1 and PCP-2, PCP-3 crystallized in space group $R\bar{3}$ with $c = 22.4756$ Å.

The compound contains one copper(II) ion, one L_1^{2-} ligand, one aqua ligand, and two solvated water molecules in the asymmetric unit (Figure S6, Supporting Information). The framework nodes also consist of binuclear copper units coordinated by the carboxylate groups of L_1^{2-} in a paddle-wheel configuration. The network is non-catenated, and there are two distinct types of metal ligand cages with D_{3d} symmetry. As shown in Figure S7 (Supporting Information), the smaller octahedral cage consists of six $[Cu_2(COO)_4]$ clusters and six L_1^{2-} ligands, whereas the larger cubo-octahedral cage is constructed of six $[Cu_2(COO)_4]$ clusters, six $[Cu_2(COO)_2]$ units and twelve L_1^{2-} ligands. The two cages are arranged in an alternating fashion along the *c* axis in a 1:1 ratio to form a cage-stacked 3D framework (**Figure 2**a). To better understand the structure of PCP-3, the binuclear copper clusters are represented as 4-connected nodes; thus the overall structure can be simplified as a uninodal 4-connected NbO net with the point (Schläfli) symbol of $\{6^4.8^2\}$ derived from TOPOS[38,39] (Figure 2b). PLATON calculation of the desolvated structure gave a porosity of 29.5%.

In order to confirm the number of guest molecules in the channels and examine the thermal stabilities of the host-frameworks, thermogravimetric analyses (TGA) were performed with freshly prepared crystals of PCPs (Figure S11, Supporting Information). TG curves showed that the paddle-wheel SBUs of PCP-1 lose the coordinated DMAc molecules at 150–275 °C, whereas for PCP-2 and PCP-3, a gradual weight loss between 30 and 150 °C is attributable to the release of both the solvated and coordinated water molecules (PCP-2: observed, 8.33%; calculated, 7.91%; PCP-3: observed, 15.17%; calculated, 14.66%). The activated materials (PCP-2′ and PCP-3′) absorbed the water vapor freely upon exposure to air, so their TGA curves also show a small amount of weight loss between 30 and 150 °C and the host-frameworks decomposed above 250 °C. The good stability provides opportunities for exploring their gas-adsorption properties.

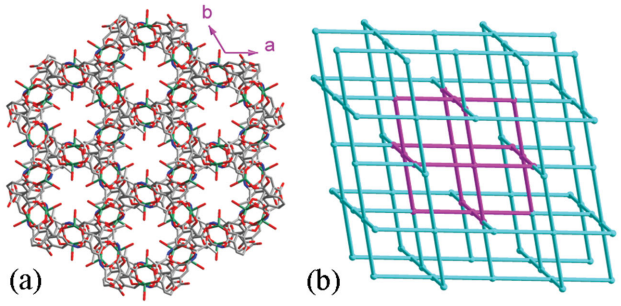

Figure 2. a) The 3D crystal framework of PCP-3. All hydrogen atoms are omitted for clarity. b) Schematic representation of the NbO network.

© 2015 WILEY-VCH Verlag GmbH & Co. KGaA, Weinheim

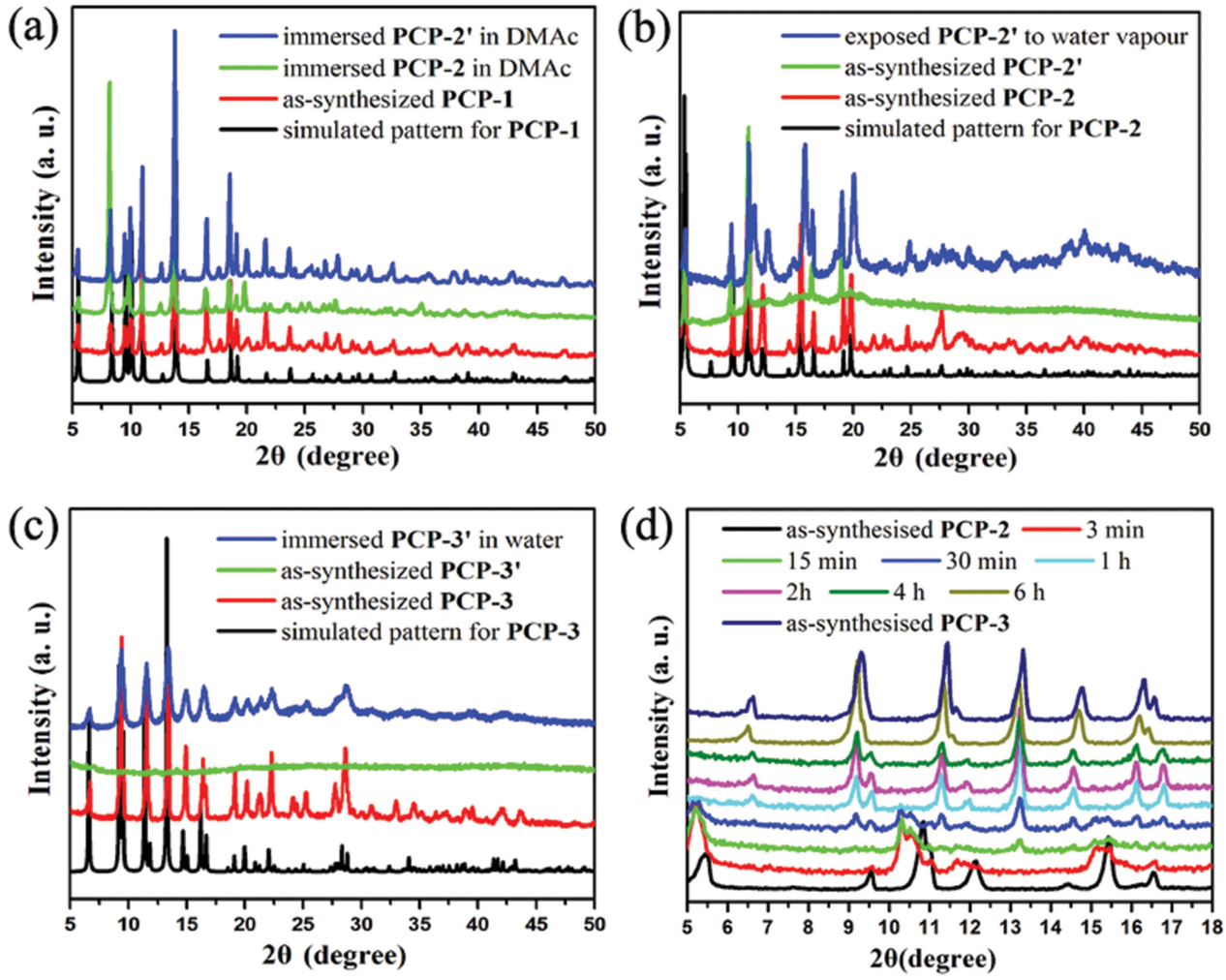

Figure 3. PXRD patterns for: a) PCP-1, b) PCP-2, c) PCP-3; d) the in situ conversion of PCP-2 to PCP-3 in the presence of water.

2.2. Powder and Single Crystal X-ray Diffraction

The bulk-phase purity of all aforementioned materials was confirmed by comparing the recorded powder X-ray diffraction (PXRD) patterns with simulated patterns from single-crystal data. All PXRD peaks of the as-synthesized PCP-1 to PCP-3 matched exactly with the respective simulated patterns (see **Figure 3**).

According to the above results, replacing the solvent ligands with water ligands can drive the single-crystal structural transformation between the source material PCP-1 and the intermediate PCP-2. As illustrated in **Scheme 2**, after the as-prepared samples of PCP-1 had been immersed in water for 10 minutes, PCP-2 could be obtained whereby the aqua ligands replaced DMAc as the terminal ligands of the binuclear copper paddle-wheel units. When PCP-1 or PCP-2 was heated at 160 °C for 5 hours, the activated PCP-2′ could be obtained. The PXRD pattern of PCP-2′ could be well indexed using the original space group $P\bar{3}$ to give unit cell parameters of a = 18.51(2) Å, c = 16.54(2) Å, V = 4908(14) Å^3 (Figure S10, Supporting Information), which is very close to those of PCP-2 (a = 18.5399(3) Å, c = 16.5649(8) Å, V = 4931.0(3) Å^3), that is, the structure of PCP-2′ should be identical with that of PCP-2 (Figure 3b). Correspondingly, PCP-1 could be recovered when PCP-2 or PCP-2′ was immersed in DMAc overnight. However, the activated PCP-2′ material also absorbed water vapor freely when exposed to air and completely transformed to PCP-2 after 30 minutes. The vacant coordination sites at the metal centers created by the removal of the solvent ligands are thus re-occupied by exposure to the ambient environment. When viewed with the naked eye, the shapes and colors of PCP-1 and PCP-2 crystals are very similar; however, the difference between the two structures can be easily distinguished from the simulated PXRD patterns (Figure S8, Supporting Information). Interestingly, the activation and re-solvation of the materials was accompanied by a color change from green (for the as-synthesized or solvent-exchanged materials) to blue (after activation), and vice versa.

Removal of the water molecules led to a significant structural change in the PCP-3 material. As shown in Figure 3c, the freshly synthesized crystalline PCP-3 changed to the amorphous state PCP-3′ after activation at high temperature. This crystalline-to-amorphous transformation was accompanied by the loss of water molecules in the channels, and this structural transformation behavior has also been observed in other

© 2015 WILEY-VCH Verlag GmbH & Co. KGaA, Weinheim

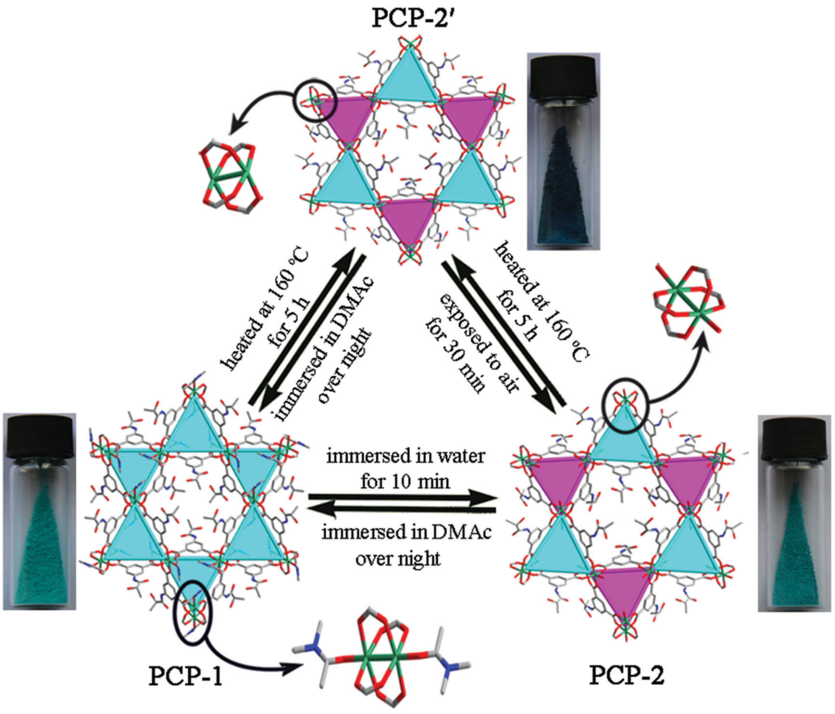

Scheme 2. Illustration of the interconversion of PCP-1 (bottom-left), PCP-2 (bottom-right), and activated PCP-2′ (top). PCP-2′ in this schematic drawing is derived from PCP-2 upon removal of the axially coordinated water molecules. The insets are photographs of the corresponding crystal materials stored in vials.

compounds.[40] Interestingly, when amorphous PCP-3′ was re-immersed in water for ten minutes, the characteristic PXRD peaks of PCP-3 could be recovered, indicating that the guest removal causes a framework distortion and partial collapse (Figure 3c). Owing to the insolubility of PCP-3′ and PCP-3 in water and taking into account the results of the vapor exposure, we can rule out the possibility of a dissolution–recrystallization process. The flexible and dynamic porous structures provided coordination sites that are suitable for the uptake of extraneous guest molecules, and are much more useful for guest selectivity than robust porous frameworks.[41]

To establish the mechanism for these guest-exchange transformations and unequivocally verify the conversion from PCP-1 to PCP-3 via the intermediate PCP-2, the reaction was monitored over time by single-crystal and powder X-ray diffraction. First, the coordinated solvent-exchange reaction during the structural transformation from PCP-1 to PCP-2 was monitored by single-crystal X-ray diffraction. The unit-cell parameters were determined after immersing a selected crystal of PCP-1 in water for various time intervals. Interestingly, this preliminary experiment indicated no change in the cell parameters (similar to PCP-1) within the first 2 minutes, which was the time required for the exchange of guest molecules. After immersion for 5 minutes, the crystal showed a lower transparency in comparison with that of the original material, and the cell parameters were very difficult to index, though the crystallinity was retained. Continued soaking for another 5 minutes resulted in unit-cell parameters that were more similar to those of PCP-2. Particularly worth mentioning is that the trigonal space group $P\bar{3}$ of the crystal remained unchanged in the whole reaction process. The diffraction spots representing typical panels were then used to follow the SCSC structural transformation process, in which the spots enclosed by triangles disappeared gradually, those shown within squares intensified with time, and those enclosed by pentagons remained constant throughout the reaction, as shown in **Figure 4**. For example, spot A denotes the {1 0 1} crystal planes with a *d* spacing of around 8.8 Å, which are present in the first 2 minutes (Figure 4a and 4b) of the process, and then disappear after 5 minutes; spot B corresponds to the equivalent {0 2 1} planes (Figure 4a and 4b) with a *d* spacing of around 6.3 Å, which gradually weakened in the first 5 minutes and then disappeared completely due to the structural rearrangement along the *c* axis; however, spot C corresponds to the {1 -2 0} planes with a *d* spacing of about 9.2 Å, which almost remained unchanged throughout the entire SCSC process, because the main change is the stacking mode from *AAAA* to *ABAB* along the *c* axis. These results clearly indicate that coordinated solvent exchange dominated at the early reaction stage because of the lack of obvious change of cell parameters; then, the sliding

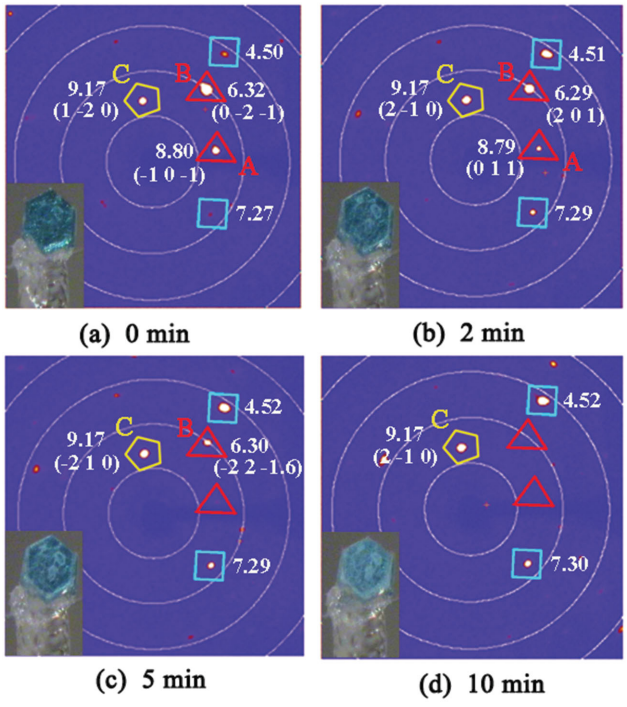

Figure 4. Diffraction patterns for crystal transformation at various time intervals after immersing a single crystal of PCP-1 in water: a) before immersion; b–d) after immersing for b) 2 minutes; c) 5 minutes; or d) 10 minutes. For easy comparison, the diffraction spots enclosed by polygons are marked with the corresponding *d* spacing/Å and Miller indices (see text).

© 2015 WILEY-VCH Verlag GmbH & Co. KGaA, Weinheim

of the layers along the *c* axis occured and finished within 10 minutes. Notably, as shown in Figure 3a, the PXRD of PCP-2 measured after immersion of one day in DMAc solution showed that the material returned to the original PCP-1 complex. In other words, the SCSC structural transformation from PCP-1 to PCP-2 represents a guest-molecule-induced reversible structural rearrangement.

Both PCP-1 and PCP-2 can be totally converted to strip-like crystals of PCP-3 after immersion in water for 6 hours. Microscopic monitoring showed that the conversion of PCP-1 to PCP-3 in the presence of water is a stepwise single-crystal to single-crystal and dissolution–recrystallization structural transformation phenomenon. As shown in Video S1 (Supporting Information), microscopic images collected at a certain time interval indicate that crystals of PCP-1 in water first lose their transparency and then the edges of the hexagon were dissolved, and finally the green strip-like crystals PCP-3 were recrystallized in situ. As illustrated in Figure 3d, the time-dependent PXRD patterns of water-treated crystals of PCP-2 showed peaks that broadened in the initial stage of the process, suggesting that the crystalline lattice of PCP-2 underwent a drastic rearrangement through the breaking and making of coordination bonds, resulting in a decrease in crystallinity owing to the structural transformation of the periodic Kagomé lattice. By extending the water-treatment time, these peaks gradually shifted to positions corresponding to the diffraction pattern of PCP-3, whereby the reaction was completed after about 6 hours.

2.3. UV–vis Spectroscopy and Proposed Mechanism

In order to further understand the process of structural transformation from PCP-2 to PCP-3, time-dependent UV–vis spectra were recorded of the isolated filtrates. For free Cu^{2+} (copper nitrate) in aqueous solution, the absorbance peak appearing at 810 nm corresponds to the d-d transition. However, the time-dependent UV–vis spectra showed a series of similar absorption peaks at 790 nm during the transformation from PCP-2 to PCP-3 (**Figure 5**a). Therefore, we speculate that the metal and ligand exist as Cu-multiligand segments in the aqueous solution during the dissolution–recrystallization process. A further study found that the intensity of the absorbance gradually increased in the first four hours, which means that dissolution occurred faster than recrystallization. However, the intensity began to decrease after the absorbance had reached its maximum, indicating that the process was reversed in the second half of the transformation (Figure 5b). The results indicate that dissolution of PCP-2 and recrystallization of PCP-3 occurred simultaneously and the Cu-multiligand fragments exist in the aqueous solution throughout the transformation process.

With reference to the phenomenon occurring in the mixed processes of single-crystal to single-crystal and dissolution–recrystallization structural transformations, we propose the following mechanism based on the hypothesis that the standard 2D Kagomé lattice PCP-1 undergoes conversion to the 3D NbO network by coordinated solvent exchange, dissolution, dissociation, distortion, reassembly, and recrystallization of the malleable $M_2(RCO_2)_4$ SBUs (**Scheme 3**). First, the presence of water leads to the exchange of the coordinated solvent to give the distorted Kagomé lattice PCP-2 structural intermediate at the beginning. When PCP-2 crystals are placed in water for a longer time, $Cu_2(RCO_2)_4$ segments dissociate and disperse into the aqueous phase. $Cu_2(RCO_2)_4$ segments of PCP-2 can twist to the $Cu_2(RCO_2)_4$ fragments of PCP-3 by the interactions with water, which is then followed by reassembly to form NbO building blocks. Ultimately, the NbO building blocks expand to the 3D PCP-3 and recrystallize from the aqueous solution. Although we acknowledge that this mechanism is only a hypothesis deduced from the experimental data, the inherent relationship between the two networks (Kagomé vs. NbO) based on similar $Cu_2(RCO_2)_4$ SBUs may offer a plausible rationale of this unique structural transformation process. The role of the solvent seems to be very important in this case. After immersing PCP-1 in lower alcohol solvents, such as methanol and ethanol, for 10 days, only the isostructures of PCP-2 were obtained (Figure S9, Supporting Information), which cannot further transform to the structure of PCP-3.

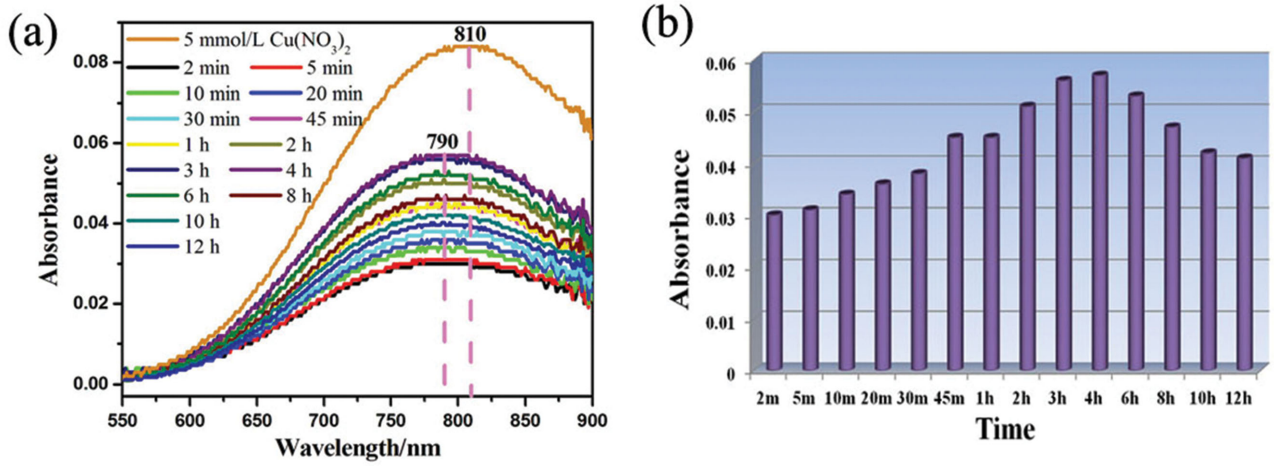

Figure 5. UV–vis spectra of the filtrate collected at different time intervals during conversion from PCP-2 to PCP-3 and comparison with free $Cu(NO_3)_2$ aqueous solution (5.00 mM).

© 2015 WILEY-VCH Verlag GmbH & Co. KGaA, Weinheim

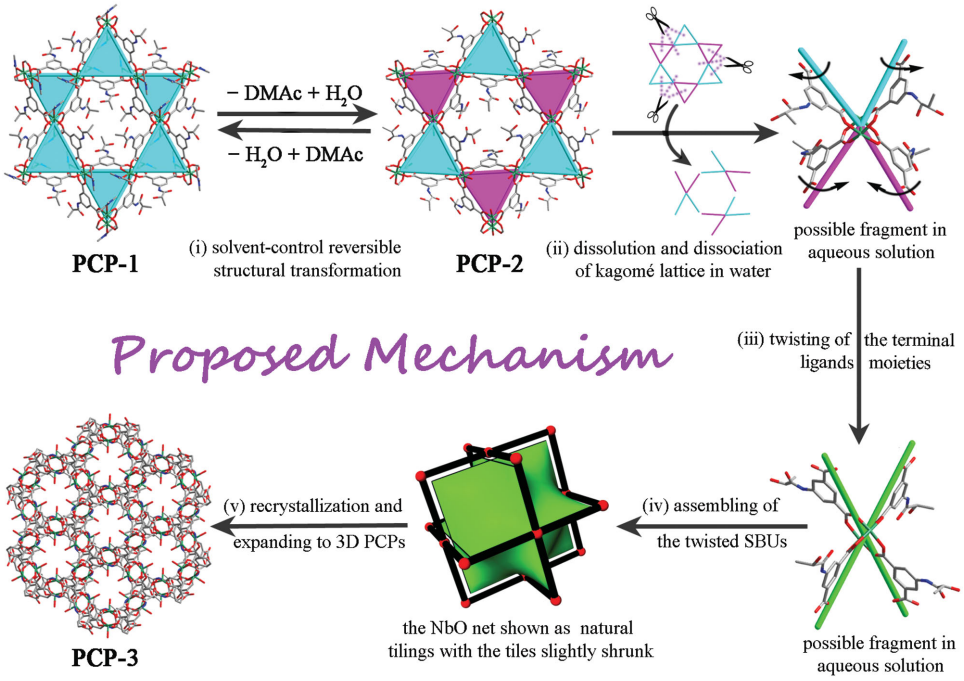

Scheme 3. Proposed mechanism for the structural transformation of the common 2D Kagomé lattice PCP-1 into the 3D NbO network PCP-3 via the structural intermediate phase PCP-2.

2.4. Sorption and Separation Properties

In light of the interesting structure–property relationships of the PCPs, we also studied their adsorption behavior for gases, including nitrogen, carbon dioxide, water, methanol, and ethanol. Although PCP-1 and PCP-2 are sensitive to liquid water, they do not transform to PCP-3 when exposed to a humid atmosphere, even if for a long time, in other words, PCP-1 and PCP-2 are moisture stable.[42] Prior to the adsorption measurements, PCP-1 and PCP-3 were activated at high temperature to remove the lattice and the coordinated guest molecules, resulting in PCP-2′ and PCP-3′, respectively. As can be seen from **Figure 6**, PCP-2′ showed almost no N_2 adsorption at 77 K but did present a type-II CO_2 adsorption at 195 K with a Langmuir surface area of 224 m^2 g^{-1}. PCP-2′ exhibited a steep uptake of CO_2 in the low-pressure region, indicating a microporosity of the activated phase. On the contrary, PCP-3′ did not adsorb CO_2 nor N_2 under the same conditions, which further confirmed that the framework collapses upon removal of the solvent molecules.

To further investigate the sorption properties of PCP-2′ and PCP-3′, water vapor adsorption measurements were also performed. As shown in **Figure 7**a, at 298 K, PCP-2′ showed a type-I adsorption isotherm profile with an uptake of 185 mL g^{-1} (14.9 wt%, 2.6 molecules per Cu^{2+}) at saturated vapor pressure, and a slight hysteresis between the adsorption and desorption isotherms was observed. The isosteric heats (Q_{st}) of adsorption were calculated by the Clausius–Clapeyron equation using isotherms measured at 283 K, 298 K, and 313 K, which could be well described by the Freundlich model (Figure S12a, Supporting Information). The values of Q_{st} were estimated to be 59.1–54.1 kJ mol^{-1} at coverages between 5 and 100 mL g^{-1} (Figure S14a, Supporting Information), which were very close to the reported values (MOF-841, ≈50 kJ mol^{-1} and MOF-801-P, ≈60 kJ mol^{-1}).[43] We also carried out water-vapor-adsorption experiments at 298 K for PCP-3′, which undergoes an interesting amorphous-to-crystalline transformation when immersed in aqueous solution. As shown in Figure 7b, the water uptake reached 251 mL g^{-1} (20.2 wt%, 3.5 molecules per Cu^{2+}) when the relative pressure was increased to 0.90. On reduction of the water vapor pressure, PCP-3′ retained water molecules, which is shown by a large

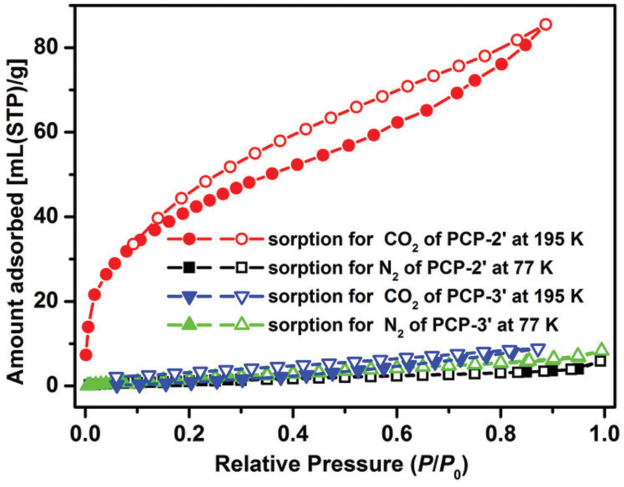

Figure 6. N_2 (77 K) and CO_2 (195 K) sorption isotherms of PCP-2′ and PCP-3′. Filled and open symbols indicate adsorption and desorption, respectively. P_0 is the saturated vapor pressure of the adsorbates at the measurement temperatures.

© 2015 WILEY-VCH Verlag GmbH & Co. KGaA, Weinheim

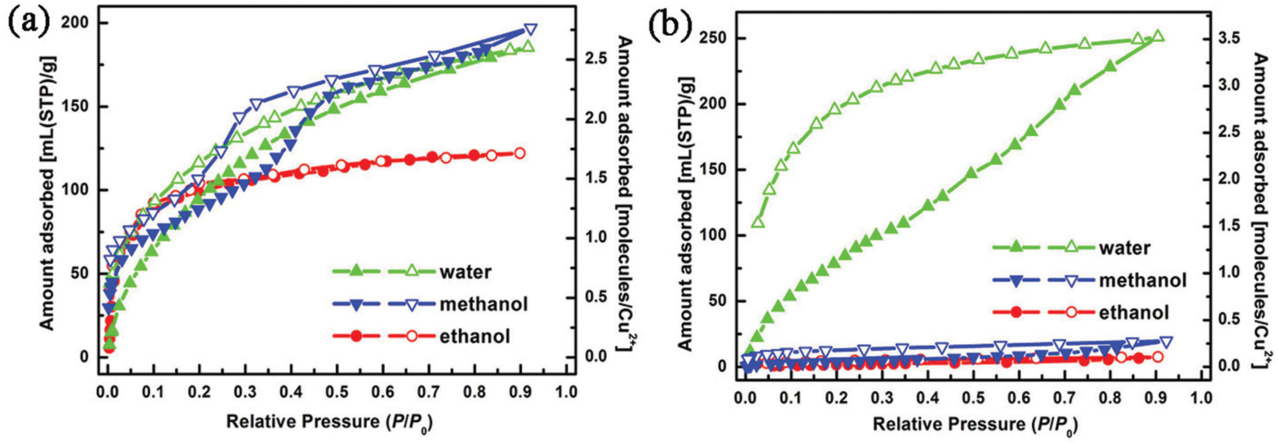

Figure 7. Adsorption isotherms of water, methanol, and ethanol for a) PCP-2′ and b) PCP-3′ at 298 K. Filled and open symbols represent adsorption and desorption data, respectively.

hysteresis between the adsorption and desorption branches. The interactions between the host framework and water were strong enough to transform and then retain the channel structure. The values of Q_{st} were estimated to be 17.3–33.6 kJ mol^{-1} at loadings between 5 and 100 mL g^{-1} (Figure S14a, Supporting Information). The general trend in the data indicates that PCP-3′ had a low Q_{st} value at the onset of adsorption, which could possibly be attributed to weaker interactions between the water molecules and the host amorphous framework. These values gradually increased until they leveled off with increasing amount of adsorbed water; in other words, the value of Q_{st} increased with flexible structural (amorphous-to-crystalline) transformations, which indicates that the water molecules have stronger interactions with crystalline PCP-3.

Interestingly, PCP-2′ adsorbs methanol and ethanol much better than PCP-3′ does. As shown in Figure 7a, the type-IV methanol-adsorption isotherm for PCP-2′ at 298 K has three distinct regions. In the first step, PCP-2′ adsorbed 75 mL g^{-1} of methanol (1.0 molecule per Cu^{2+}) before $P/P_0 = 0.1$, and then 80 mL g^{-1} of additional methanol was adsorbed when P/P_0 was increased up to 0.5. Finally the total adsorbed amount of methanol was 197 mL g^{-1} (28.2 wt%, 2.76 molecules per Cu^{2+}) at $P/P_0 = 0.92$. For ethanol adsorption of PCP-2′ at 298 K, the isotherm belongs to a type-I profile similar to that of water-vapor adsorption. Ethanol was also rapidly adsorbed into PCP-2′ in the low-pressure region, and the ethanol uptake increased as the vapor pressure increased. Finally, 106 mL g^{-1} (21.8 wt%, 1.49 molecules per Cu^{2+}) of ethanol was adsorbed at saturated vapor pressure, and no obvious hysteresis between the adsorption and desorption isotherms was observed. We extrapolated the heats of adsorption for PCP-2′, and found that for methanol adsorption the heats of adsorption were low at low loading value, and increased with the amount of adsorption at coverages between 5 and 70 mL g^{-1} (Figure S14b, Supporting Information). The ethanol-adsorption isotherms could be well fitted using the Langmuir equation (Figure S13b, Supporting Information). The value of Q_{st} also showed an upward trend with increased loading. On the contrary, for PCP-3′, only negligible amounts of methanol and ethanol uptake were detected under similar experimental conditions (Figure 7b). Because of the conversion of the amorphous to the crystalline phase, PCP-3′ showed a highly selective adsorption for water over alcohols. This ultraselective adsorption of water by PCP-3′ over methanol and ethanol is particularly noteworthy and makes it an excellent candidate material for water/alcohol separation.

3. Conclusion

We report a dramatic water-triggered diplex structural transformation involving both single-crystal to single-crystal and dissolution–recrystallization processes from a standard 2D Kagomé lattice to a 3D NbO network via a distorted Kagomé lattice structural intermediate. This process was fully demonstrated by single-crystal crystallography, powder X-ray diffraction, and UV–vis spectral measurements. The isolation and characterization of a structural intermediate was crucial for the ability to propose the mechanism for the dynamic structural transformation and was also important for understanding the structure–property relationships. Moreover, the activated materials PCP-2′ and PCP-3′ exhibited different gas-adsorption properties, whereby PCP-3′ was highly selective for water adsorption and is therefore expected to be an excellent candidate material for water/alcohol separation. We believe that these findings not only provide an insight into understanding the intrinsic mechanism of the structural transformation process, but also furnish a particular viewpoint to realize structure–property relationships in crystalline materials.

4. Experimental Section

Materials and General Methods: All starting solvents and materials were obtained from commercial vendors, unless otherwise specified, and were used without further purification. ^{1}H-NMR spectra were recorded on a Bruker-400 spectrometer and the chemical shifts were reported in ppm using tetramethylsilane (TMS) as the internal standard. The Fourier-transform infrared (FT-IR) spectra were obtained in the range of 4000–400 cm^{-1} on KBr pellet samples on a Bruker VECTOR 22 spectrometer. Elemental analyses for C, H, and N were carried out on

© 2015 WILEY-VCH Verlag GmbH & Co. KGaA, Weinheim

a Perkin-Elmer 240 elemental analyzer. Powder X-ray diffraction (PXRD) data were measured at 293 K on a Rigaku D/max-3B diffractometer (Cu Kα, λ = 1.5418 Å). The crushed single-crystalline powder samples were prepared by crushing the crystals and scanning them from 5 to 50° with a step of 0.1° s^{-1}. Thermal analyses were performed on a SDT 2960 thermal analyzer using temperatures from room temperature to 600 °C at a heating rate of 10 °C min^{-1} under air atmosphere. UV–vis absorption spectra were measured with a TU-1901 double-beam UV–vis spectrophotometer. Adsorption of various vapors on the samples were investigated on a Micromeritics 3FLEX adsorption apparatus. The experimental temperatures were maintained by using liquid nitrogen (77 K), dry ice–acetone baths (195 K), and temperature-programmed water baths (283, 298, and 313 K), respectively.

5-(2-Acetoxy-propionylamino)-isophthalic acid (H_2L): The H_2L ligand was prepared by the reaction of 2-acetoxypropionyl chloride with 5-amino-isophthalic acid (Scheme S1, Supporting Information). 2-acetoxypropionyl chloride was synthesized according to the literature.[44] 2-acetoxypropionyl chloride (6.30 mL, 49.5 mmol) was added drop-wise to a solution of 5-amino-isophthalic acid (3 g, 16.5 mmol) in DMAc (20 mL). The resulting mixture was stirred at about 50 °C for 5.5 h. Distilled water (80 mL) was added to the reaction mixture at room temperature, and cooled to a temperature between 0 °C and 5 °C and stirred for 30 minutes at this low temperature. The precipitate was filtered and the filter cake was washed with distilled water. The product was dried overnight in a vacuum oven at 60 °C to yield H_2L (3.93 g, 13.3 mmol, 80.6%). ^{1}H NMR (400 MHz, DMSO-d_6, δ): 13.28 (s, 2H), 10.44 (s, 1H), 8.45 (s, 2H), 8.18 (s, 1H), 5.04 (m, 1H), 2.11 (s, 3H), 1.45(d, 3H); IR (KBr): ν = 3278 (m), 1744 (s), 1692 (vs), 1605 (w), 1556 (s), 1440 (w), 1408 (m), 1369 (w), 1282 (s), 1234 (s), 1105 (m), 1050 (w), 948 (w), 913 (w), 757 (m), 692 (m), 607 (w), 538 (w), 494 cm^{-1} (w). Anal. calcd. for $C_{13}H_{13}O_7N$: C 52.88, H 4.44, N 4.74; found: C 53.21, H 4.09, N 4.91.

5-(2-Hydroxy-propionylamino)-isophthalic acid (H_2L_1): H_2L (3.0 g, 10.0 mmol) was dissolved in 60 mL of methanol with a stoichiometric amount of CH_3ONa and the mixture was stirred for 20 h at room temperature. Subsequently, Amberlyst 15 (ion-exchange resin, 3.6 g) was added and stirred for 2 h. After filtration, 2 g Amberlyst 15 was added and stirred for another 2 h. After filtration, the solution was evaporated under reduced pressure, and the resulting off-white solid H_2L_1 was dried under vacuum overnight. Yield: 2.33 g, 9.21 mmol, 92%. ^{1}H NMR: (400 MHz, DMSO-d_6, δ): 10.00 (s, 1H), 8.42 (s, 2H), 8.20 (s, 1H), 4.18 (m, 1H), 1.32(d, 3H); IR (KBr): ν = 3423 (s), 1686 (m), 1607 (s), 1572 (vs), 1430 (m), 1371 (m), 1260 (m), 1119 (m), 1048 (w), 950 (w), 902 (w), 770 (w), 560 (w), 475 cm^{-1} (w). Anal. calcd. for $C_{11}H_{11}O_6N$: C 52.18, H 4.38, N 5.53; found: C 52.83, H 3.99, N 5.21.

Synthesis of $[Cu(L_1)(DMAc)]_n$ (PCP-1): H_2L (295 mg, 1.0 mmol) and $Cu(NO_3)_2{\cdot}3H_2O$ (241 mg, 1.0 mmol) were dissolved in a mixture of DMAc and water (2:1, 15 mL) in a Teflon-lined stainless steel vessel (25 mL). The solution was heated in an oven at 90 °C for 3000 minutes, and then cooled to room temperature. Green hexagonal flake crystals (PCP-1) which were suitable for single-crystal X-ray analysis were obtained by filtration. The obtained crystals were washed with a fresh mixture of DMAc and water (yield: 90% based on copper) and dried in air. The resulting formula was derived from crystallographic data, elemental analysis, and TGA (Figure S11, Supporting Information). IR (KBr): ν = 3423 (m), 1617 (s), 1590 (s), 1417 (m), 1376 (vs), 1246 (w), 1119 (w), 1047 (m), 910 (w), 777 (w), 730 (w), 494 cm^{-1} (w). Anal. calcd. for $C_{15}H_{18}CuN_2O_7$: C 44.83, H 4.52, N 6.97; found: C 44.47, H 5.03, N 7.15.

Synthesis of $\{[Cu_2(L_1)_2(H_2O)_2]{\cdot}H_2O\}_n$ (PCP-2): PCP-1 (300 mg) was placed in a 25 mL vial, water (10 mL) was added, and the resulting mixture was standing at room temperature for 10 minutes. The green hexagonal flake crystals were filtered and washed with distilled water (yield of the isolated product: 100%). The crystals were characterized after drying at room temperature. The formula of PCP-2 is $\{[Cu_2(L_1)_2(H_2O)_2]{\cdot}H_2O\}_n$, which was derived from crystallographic data, elemental analysis, and TGA (Figure S11, Supporting Information). IR (KBr): ν = 3419 (m), 1616 (m), 1590 (s), 1417 (m), 1376 (vs), 1242 (w), 1112 (w), 1047 (w), 906 (w), 777 (m), 730 (m), 492 cm^{-1} (w). Anal. calcd. for $C_{22}H_{24}Cu_2N_2O_{15}$: C 38.66, H 3.54, N 4.10; found: C 39.17, H 3.64, N 3.98.

Synthesis of $\{[Cu(L_1)(H_2O){\cdot}2H_2O]\}_n$ (PCP-3): PCP-1 or PCP-2 (300 mg) was placed in a 25 mL vial, water (10 mL) was added, and the resulting mixture was left to stand at room temperature for 6 hours. The green strip-like crystals that formed were filtered and washed with distilled water (yield of the isolated product: 70%). The crystals were characterized after drying at room temperature. The formula of PCP-3 is $\{[Cu(L_1)(H_2O){\cdot}2H_2O]\}_n$, which was derived from crystallographic data, elemental analysis, and TGA (Figure S11, Supporting Information). IR (KBr): ν = 3373 (s), 1626 (s), 1559 (vs), 1417 (s), 1376 (vs), 1251 (w), 1119 (w), 1048 (m), 905 (w), 779 (m), 730 (m), 495 cm^{-1} (w). Anal. calcd. for $C_{11}H_{15}CuNO_9$: C 35.82, H 4.10, N 3.80; found: C 35.47, H 4.15, N 3.28.

Synthesis of PCP-2′ and PCP-3′: PCP-1 or PCP-2 (200 mg) was heated at 433 K in an oven or activated at 393 K under a dynamic vacuum for 5 hours; the activated PCP-2′ was obtained. Similarly, PCP-3 (200 mg) was heated at 413 K in an oven or activated at 373 K under a dynamic vacuum for 5 hours, and then the activated PCP-3′ was obtained.

[CCDC 1407352-1407354 contains the supplementary crystallographic data for this paper. These data can be obtained free of charge from The Cambridge Crystallographic Data Centre via www.ccdc.cam.ac.uk/data_request/cif.]

Supporting Information

Supporting Information is available from the Wiley Online Library or from the author.

Acknowledgements

This work was supported by the National Natural Science Foundation of China (No. 21371153, 20901070) and the Program for Science & Technology Innovation Talents in the Universities of Henan Province (13HASTIT008), the Key Scientific and Technological Project of Henan Province (132102210411), and Zhengzhou University.

Received: July 29, 2015
Revised: August 24, 2015
Published online: September 21, 2015

[1] a) J. R. Long, O. M. Yaghi, *Chem. Soc. Rev.* **2009**, *38*, 1213; b) H.-C. Zhou, J. R. Long, O. M. Yaghi, *Chem. Rev.* **2012**, *112*, 673; c) H.-C. Zhou, S. Kitagawa, *Chem. Soc. Rev.* **2014**, *43*, 5415.
[2] a) S. Kitagawa, R. Kitaura, S.-i. Noro, *Angew. Chem. Int. Ed.* **2004**, *43*, 2334; b) M. B. Duriska, S. M. Neville, J. Lu, S. S. Iremonger, J. F. Boas, C. J. Kepert, S. R. Batten, *Angew. Chem. Int. Ed.* **2009**, *48*, 8919.
[3] Z. R. Herm, B. M. Wiers, J. A. Mason, J. M. van Baten, M. R. Hudson, P. Zajdel, C. M. Brown, N. Masciocchi, R. Krishna, J. R. Long, *Science* **2013**, *340*, 960.
[4] a) J. Y. Lee, L. Pan, X. Huang, T. J. Emge, J. Li, *Adv. Funct. Mater.* **2011**, *21*, 993; b) S.-Y. Liu, X.-L. Qi, R.-B. Lin, X.-N. Cheng, P.-Q. Liao, J.-P. Zhang, X.-M. Chen, *Adv. Funct. Mater.* **2014**, *24*, 5866.
[5] T. Hang, W. Zhang, H.-Y. Ye, R.-G. Xiong, *Chem. Soc. Rev.* **2011**, *40*, 3577.
[6] G. K. H. Shimizu, J. M. Taylor, S. Kim, *Science* **2013**, *341*, 354.

© 2015 WILEY-VCH Verlag GmbH & Co. KGaA, Weinheim

[7] a) S. R. Batten, R. Robson, *Angew. Chem. Int. Ed.* **1998**, *37*, 1460; b) A. Schoedel, L. Wojtas, S. P. Kelley, R. D. Rogers, M. Eddaoudi, M. J. Zaworotko, *Angew. Chem. Int. Ed.* **2011**, *50*, 11421.
[8] a) L. Brammer, *Chem. Soc. Rev.* **2004**, *33*, 476; b) M. Eddaoudi, D. F. Sava, J. F. Eubank, K. Adil, V. Guillerm, *Chem. Soc. Rev.* **2015**, *44*, 228.
[9] Y. He, B. Li, M. O'Keeffe, B. Chen, *Chem. Soc. Rev.* **2014**, *43*, 5618.
[10] V. Guillerm, D. Kim, J. F. Eubank, R. Luebke, X. Liu, K. Adil, M. S. Lah, M. Eddaoudi, *Chem. Soc. Rev.* **2014**, *43*, 6141.
[11] S. Horike, S. Shimomura, S. Kitagawa, *Nat. Chem.* **2009**, *1*, 695.
[12] A. Schneemann, V. Bon, I. Schwedler, I. Senkovska, S. Kaskel, R. A. Fischer, *Chem. Soc. Rev.* **2014**, *43*, 6062.
[13] a) P. K. Allan, B. Xiao, S. J. Teat, J. W. Knight, R. E. Morris, *J. Am. Chem. Soc.* **2010**, *132*, 3605; b) N. Yanai, T. Uemura, M. Inoue, R. Matsuda, T. Fukushima, M. Tsujimoto, S. Isoda, S. Kitagawa, *J. Am. Chem. Soc.* **2012**, *134*, 4501.
[14] L. Wen, P. Cheng, W. Lin, *Chem. Commun.* **2012**, *48*, 2846.
[15] C.-T. He, P.-Q. Liao, D.-D. Zhou, B.-Y. Wang, W.-X. Zhang, J.-P. Zhang, X.-M. Chen, *Chem. Sci.* **2014**, *5*, 4755.
[16] D. Bradshaw, J. E. Warren, M. J. Rosseinsky, *Science* **2007**, *315*, 977.
[17] Y.-C. Ou, D.-S. Zhi, W.-T. Liu, Z.-P. Ni, M.-L. Tong, *Chem. Eur. J.* **2012**, *18*, 7357.
[18] a) G. K. Kolea, J. J. Vittal, *Chem. Soc. Rev.* **2013**, *42*, 1755; b) R. Medishetty, R. Tandiana, J. Wu, Z. Bai, Y. Du, J. J. Vittal, *Chem. Eur. J.* **2015**, *21*, 11948.
[19] P.-Q. Liao, A.-X. Zhu, W.-X. Zhang, J.-P. Zhang, X.-M. Chen, *Nat. Commun.* **2015**, *6*, 6350.
[20] G. M. Espallargas, J. van de Streek, P. Fernandes, A. J. Florence, M. Brunelli, K. Shankland, L. Brammer, *Angew. Chem. Int. Ed.* **2010**, *49*, 8892.
[21] I. J. Vitóica-Yrezábal, S. Libri, J. R. Loader, G. M. Espallargas, M. Hippler, A. J. Fletcher, S. P. Thompson, J. E. Warren, D. Musumeci, M. D. Ward, L. Brammer, *Chem. Eur. J.* **2015**, *21*, 8799.
[22] X. Cui, A. N. Khlobystov, X. Chen, D. H. Marsh, A. J. Blake, W. Lewis, N. R. Champness, C. J. Roberts, M. Schröder, *Chem. Eur. J.* **2009**, *15*, 8861.
[23] X.-F. Wang, Y. Wang, Y.-B. Zhang, W. Xue, J.-P. Zhang, X.-M. Chen, *Chem. Commun.* **2012**, *48*, 133.
[24] S. Kitagawa, R. Matsuda, *Coord. Chem. Rev.* **2007**, *251*, 2490.
[25] a) S. K. Ghosh, W. Kaneko, D. Kiriya, M. Ohba, S. Kitagawa, *Angew. Chem. Int. Ed.* **2008**, *47*, 8843; b) H. Sato, W. Kosaka, R. Matsuda, A. Hori, Y. Hijikata, R. V. Belosludov, S. Sakaki, M. Takata, S. Kitagawa, *Science* **2014**, *343*, 167.
[26] a) H. Aggarwal, P. Lama, L. J. Barbour, *Chem. Commun.* **2014**, *50*, 14543; b) H. Aggarwal, R. K. Das, P. M. Bhatt, L. J. Barbour, *Chem. Sci.* **2015**, *6*, 4986.
[27] a) X.-Z. Song, S.-Y. Song, S.-N. Zhao, Z.-M. Hao, M. Zhu, X. Meng, L.-L. Wu, H.-J. Zhang, *Adv. Funct. Mater.* **2014**, *24*, 4034; b) M. Zhu, X.-Z. Song, S.-Y. Song, S.-N. Zhao, X. Meng, L.-L. Wu, C. Wang, H.-J. Zhang, *Adv. Sci.* **2015**, *2*, 1500012.
[28] J.-P. Zhang, P.-Q. Liao, H.-L. Zhou, R.-B. Lin, X.-M. Chen, *Chem. Soc. Rev.* **2014**, *43*, 5789.
[29] A. Mallick, B. Garai, D. D. Díaz, R. Banerjee, *Angew. Chem. Int. Ed.* **2013**, *52*, 13755.
[30] P. Shen, W.-W. He, D.-Y. Du, H.-L. Jiang, S.-L. Li, Z.-L. Lang, Z.-M. Su, Q. Fu, Y.-Q. Lan, *Chem. Sci.* **2014**, *5*, 1368.
[31] S. B. Choi, H. Furukawa, H. J. Nam, D. Y. Jung, Y. H. Jhon, A. Walton, D. Book, M. O'Keeffe, O. M. Yaghi, J. Kim, *Angew. Chem. Int. Ed.* **2012**, *51*, 8791.
[32] Q. Chen, Z. Chang, W.-C. Song, H. Song, H.-B. Song, T.-L. Hu, X.-H. Bu, *Angew. Chem. Int. Ed.* **2013**, *52*, 11550.
[33] A. Shigematsu, T. Yamada, H. Kitagawa, *J. Am. Chem. Soc.* **2012**, *134*, 13145.
[34] D.-X. Xue, Y. Belmabkhout, O. Shekhah, H. Jiang, K. Adil, A. J. Cairns, M. Eddaoudi, *J. Am. Chem. Soc.* **2015**, *137*, 5034.
[35] R. Plessius, R. Kromhout, A. L. D. Ramos, M. Ferbinteanu, M. C. Mittelmeijer-Hazeleger, R. Krishna, G. Rothenberg, S. Tanase, *Chem. Eur. J.* **2014**, *20*, 7922.
[36] T. Yamada, H. Kitagawa, *J. Am. Chem. Soc.* **2009**, *131*, 6312.
[37] A. L. Spek, *J. Appl. Crystallogr.* **2003**, *36*, 7.
[38] V. A. Blatov, A. P. Shevchenko, V. N. Serezhkin, *J. Appl. Crystallogr.* **2000**, *33*, 1193.
[39] V. A. Blatov, M. V. Peaskov, *Acta Crystallogr. B: Struct. Sci.* **2006**, *62*, 457.
[40] D. Maspoch, D. Ruiz-Molina, K. Wurst, N. Domingo, M. Cavallini, F. Biscarini, J. Tejada, C. Rovira, J. Veciana, *Nat. Mater.* **2003**, *2*, 190.
[41] S. Kitagawa, K. Uemura, *Chem. Soc. Rev.* **2005**, *34*, 109.
[42] J. Canivet, A. Fateeva, Y. Guo, B. Coasne, D. Farrusseng, *Chem. Soc. Rev.* **2014**, *43*, 5594.
[43] H. Furukawa, F. Gándara, Y.-B. Zhang, J. Jiang, W. L. Queen, M. R. Hudson, O. M. Yaghi, *J. Am. Chem. Soc.* **2014**, *136*, 4369.
[44] a) K. N. Slessor, G. G. S. King, D. R. Miller, M. L. Winston, H. Cutforth, *J. Chem. Ecol.* **1985**, *11*, 1659; b) R. Hulst, N. K. de Vries, B. L. Feringa, *Tetrahedron* **1994**, *50*, 11721.

© 2015 WILEY-VCH Verlag GmbH & Co. KGaA, Weinheim